Characterization and Application of Nanomaterials (2021) Volume 4 Issue 1
doi:10.24294/can.v4i1.996

ORIGINAL RESEARCH ARTICLE

A theoretical study of (9, 0) Singlewalled Carbon Nanotubes using quantum mechanical techniques

Deepa Sharma[1*], Neena Jaggi[2]

[1] *SUS Govt. College, Matak-Majri (Indri), Haryana-India. E-mail: bhargava.dp@gmail.com*

[2] *National Institute of Technology, Kurukshetra-(Haryana)-India*

ABSTRACT

First principles simulation studies using the density functional theory have been performed on (9, 0) Zigzag Singlewalled Carbon Nanotube (SWCNT) to investigate its electronic, optical and thermodynamic properties using CASTEP (Cambridge Sequential Total Energy Package) and DFTB (Density Functional based Tight Binding) modules of the Material Studio Software version 7.0. Various functionals and sub-functionals available in the CASTEP Module (using Pulay Density Mixing treatment of electrons) and various eigen-solvers and smearing schemes available in the DFTB module (using smart algorithm) have been tried out to chalk out the electronic structure. The analytically deduced values of the band gap obtained were compared with the experimentally determined value reported in the literature. By comparison, combination of Anderson smearing scheme and standard diaogonalizer produced best results in DFTB module while in the CASTEP module, GGA (General Gradient approximation) functional with RPBE (Revised-per-dew-Burke-Ernzerh) as Sub-functional was found to be the most consistent. These optimized parameters were then used to determine various electronic, optical and thermodynamic properties of (9, 0) Singlewalled Nanotube. (9, 0) Singlewalled Nanotube, which is extensively being used for sensing NH_3, CH_4 & NO_2, has been picked up in particular as it is reported to exhibit a finite energy band gap in contrast to its expected metallic nature. The study is of utmost significance as it not only probes and validates the simulation route for predicting suitable properties of nanomaterials but also throws light on the comparative efficacy of the different approximation and rationalization quantum mechanical techniques used in simulation studies.

Keywords: Simulation; Density Functional Theory; Molecular Modeling; CASTEP; DFTB; SWCNT

ARTICLE INFO

Received: 26 December 2020
Accepted: 12 February 2021
Available online: 21 February 2021

1. Introduction

Since the advent of Carbon Nanotubes by Iijima in 1991[1] and subsequent synthesis of Singlewalled Carbon Nanotubes (SWCNTs) by Iijima[2] & Bethune[3], Singlewalled Carbon Nanotubes have grabbed utmost attention because of their mesmerizing electrical[4,5], mechanical[6,7] and optical properties[8,9]. This multifaceted seamless one-dimensional roll of a single layer of graphite (graphene) has revealed highly promising applications in future molecular electronics[10,11] over the last few decades. The remarkable electronic properties of these 1-D structures make them suitable for various applications in nanotechnology, optics, electronics, and other fields of materials science as chemical sensors[12–19], actuators[20], nano biomaterial[21,22], conductive heating film[23,24], conductive transparent electrode[25,26], conductive nanoink[27], nano device[28–32], and display (backlight, flat lamp and field emitter)[32,33] etc. This has invoked interest in the experimentalists as well as theore-

ticians. Experimentalists are trying to develop new methods of synthesizing, purifying and functionalizing SWCNTs and exploring possibilities of their use into new devices and applications. On the other hand, theoreticians are implying theory and computational modeling to determine the structural, mechanical, thermal and electronic behaviour with accuracy by using computational nanotechnology. The simulation techniques are being used for predictions. Various concepts and designs have been theoretically evolved through modeling and simulation and then realized or verified experimentally[34].

In this paper, the electronic structure of a (9, 0) SWCNT has been investigated using DFTB & CASTEP modules of the Material Studio Software version 7.0, and relative efficacy of various functionals and subfunctionals has been compared and electronic, optical and thermodynamic properties have been studied using the optimum combination of the functional & sub-functional and diagonalization technique & density mixing scheme. The motive behind choosing (9, 0) SWCNT as the target material has on the one hand been its current extensive application as a gas sensor for the poisonous gases like NH_3[12], CH_4[13] and NO_2[14]. On the other hand, the reported finite band gap in contrast to the expected metallic nature also served as a driving force for this study.

2. Theory

Beginning with the bottom-up, a few tens to hundreds of atoms can be simulated using quantum mechanics based first principle methods, which involve the solution of the complex quantum of many body by Schrödinger equation of the atomic system using different computational algorithms[35]. The atoms are treated as a group of quantum mechanical particles governed by the Schrödinger equation:

$$\hat{H}\psi = E\psi$$

Where, $\hat{H}$ is the many-body Hamiltonian operator. However, with Born-Oppenheimer approximation, a many body problem is reduced to a many electron problem. Current first principle methods are based on the density functional theory (DFT)[36,37]. DFT is based on the concept that the ground state total electronic energy is a unique functional of the density of the system. Kohn and Sham[36,37] have shown that the DFT can be reduced to a single electron problem with self-consistent effective potential, which takes into consideration the exchange correlation effects of the interactions of the electrons. This reformulation of Schrödinger equation into a single electron problem is known as Kohn-Sham equation. Many approximations like local density approximation (LDA), general gradient approximation (GGA), Hartree Fock approximation (HF), Hartee Fock-local density approximation (HF-LDA), etc[34–47]. were proposed to approximate the effective exchange-correlation potential[36,40]. To be more specific, certain sub-functional are associated with the approximation functional like LDA, CA-PZ, GGA-PBE, GGA-RPBE, GGA-PW91, GGA-WC, GGA-PBESOL, etc[34–47]. These approximation based first principles methods have been successful in various modeling and simulation tasks planned for structural, chemical & electronic characterization of nanomaterials. For practical applications, these simulation methods are implemented with a pseudo-potential approximation (ultrasoft, normconserving or on the fly) and a plane wave basis expansion of single electron wavefunctions[47]. These approximations convert the electronic structure problem into a self-consistent matrix diagonalization problem[34,45,46]. When the iterative matrix diagonalization procedure completes, the eigen values obtained correspond to energy states of the system. The eigen functions provide information about the electronic density distribution. CASTEP (Cambridge Sequential Total Energy Package) and DFTB (Density Functional Tight Binding) are immensely effective DFT simulation programs available through Accelrys Material Studio Software as user-friendly modules through a license agreement[47].

3. Computational details

This paper elaborates first principles investigations on a zigzag Singlewalled Carbon Nanotube with chirality (9, 0) using the software Material Studio version 7.0 installed on an 8 core Intel(R) Core(TM) i7-3770 CPU @ 3.40 GHz with Windows

operating system. To start with, structural unit was simulated via molecular modelling, which comprised of 144 electrons in the 36 carbon atoms of the specific nanotube giving rise to 87 energy bands in its electronic band structure. The band gap studies were performed using CASTEP as well as DFTB Modules.

Initially the task was set up using DFTB module. Static calculations were performed with self-consistent charges using the smart algorithm. Different combinations of diagonalization techniques (standard/divide & conquer) and smearing schemes (Anderson/Broyden/DIIS/linear) were tried. Suitable choice of various tolerance parameters is very crucial for geometry optimization. The same task was then set up using CASTEP Module. The structure of the CNT was first electronically minimized through pseudo-atomic calculations using LDA(CA-PZ) , GGA(RPBE), GGA(WC), GGA(PW91), GGA(PBESOL) functionals with Pulay density mixing treatment of the electrons, choosing a suitable cut-off energy & tolerance values for various parameters like energy, maximum force, maximum stress, maximum displacement, charge spilling parameter etc. Ultrasoft pseudo-potential was used in the reciprocal lattice with fixed basis set quality using Gaussian smearing scheme with suitably chosen smearing width without any periodic dipole correction. BFGS algorithm which implements variable cell method with geometry line minimiser was initiated to calculate the ground state eigen values, eigen functions and density. Continuing with the ground state wavefunction thus determined and ground state density thus calculated, general k-point calculations for band structure and density of states were performed.

In comparison with the experimental results, the calculation performed in CASTEP module with GGA (RPBE) and the calculation performed in DFTB module with standard diagonalizer & Anderson smearing scheme were found to deliver the best match. Hence thereafter, electronic, optical and thermodynamic studies were performed using the same combination of functional & sub-functional.

4. Results and discussions

4.1 Geometry optimization

4.1.1 DFTB module

While performing static calculations with self-consistent charges for geometry optimization using the smart eigen-solver in the DFTB module, different combinations of diagonalization techniques (standard, divide & conquer) and mixing schemes (Anderson, Broyden, DIIS & linear) were tried keeping SCC tolerance value at 0.1×10^4, energy tolerance value at 0.05 kcal/mol, force tolerance value at 0.05 kcal/mol/A^o and Ewald alpha parameter ≈ 0.22 (**Figure 1**).

The optimization process was carried out with respect to the parameters like energy change, force constant and normal stress component (**Figure 2a**) and converged at different energies for different mixing schemes & diagonalization techniques, finally leading to an optimized hexagonal geometry (**Figures 2b** & **2c**).

In all the tasks set up using DFTB, thermal smearing with smearing parameter 0.005 Hartree was used without any dipole correction. The results obtained may be summarized as follows:

Table 1. DFTB Geometry optimization: (9, 0) Singlewalled Carbon Nanotube

Mixing Scheme / Parameter	Standard diagonalization				Divide & conqure diagonalization			
	Anderson	**Broyden**	**Diis**	**Linear**	**Anderson**	**Broyden**	**Diis**	**Linear**
Total energy (Hartree)	–61.84978	–61.57981	–61.57979	–61.57985	–61.57981	–61.57981	–61.57979	–61.57985
Total enthalpy (kcal/mol)	–38777.3	–38598.7	–38598.7	–38598.7	–38598.7	–38598.7	–38598.7	–38598.7
Free energy (Hartree)	–61.85235	–61.58217	–61.58217	–61.58215	–61.58216	–61.58217	–61.58217	–61.58215
Volume $(A^0)^3$	0.288×10^4	0.269×10^4	0.269×10^4	0.269×10^4	0.269×10^4	0.269×10^4	0.269×10^4	0.269×10^4
Pressure (-Pa)	0.260×10^8	0.139×10^8	0.054×10^8	0.511×10^8	0.082×10^8	0.139×10^8	0.054×10^8	0.511×10^8
rms force (kcal/mol/A^0)	7.479	8.573	8.573	8.573	8.573	8.573	8.573	8.573
Max. force (kcal/mol/A^0)	12.90	14.69	14.69	14.69	14.69	14.69	14.69	14.69
rms stress (GPa)	88.59	95.10	95.10	95.10	95.10	95.10	95.10	95.10
Max. stress (GPa)	167.6	184.3	184.3	184.3	184.3	184.3	184.3	184.3

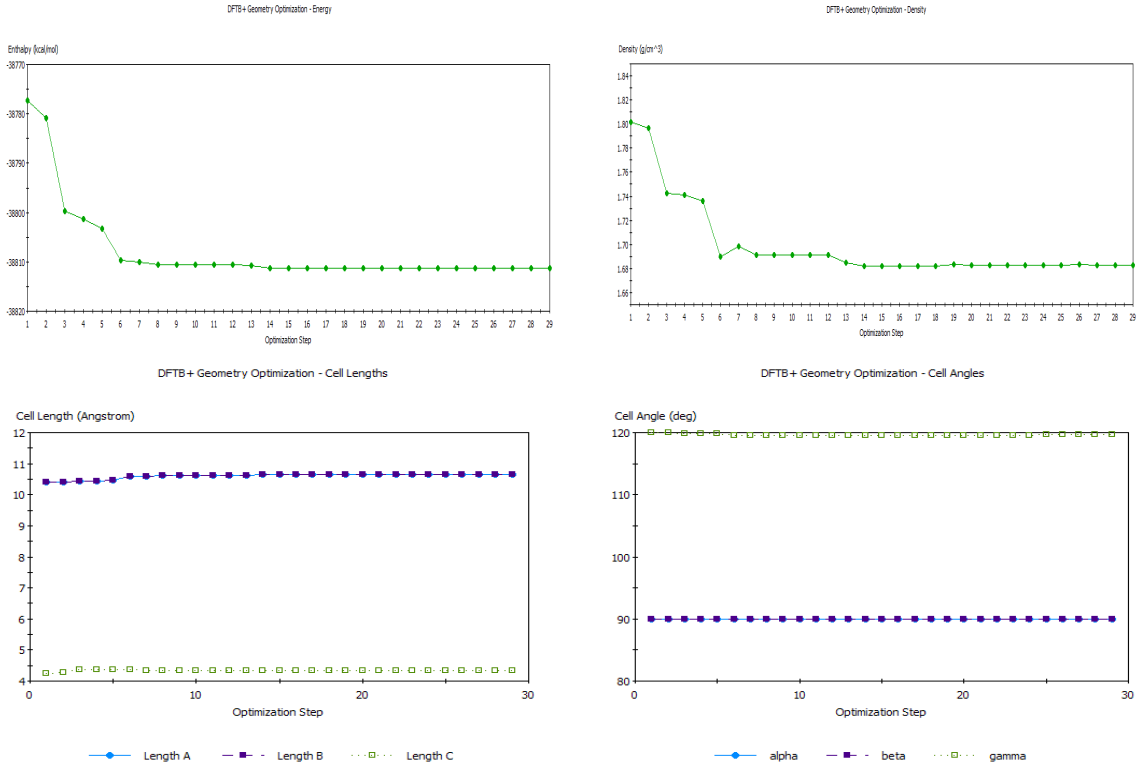

Figure 1. DFTB Geometry optimization w.r.t. **a)** energy **b)** density **c)** cell lengths & **d)** cell angles.

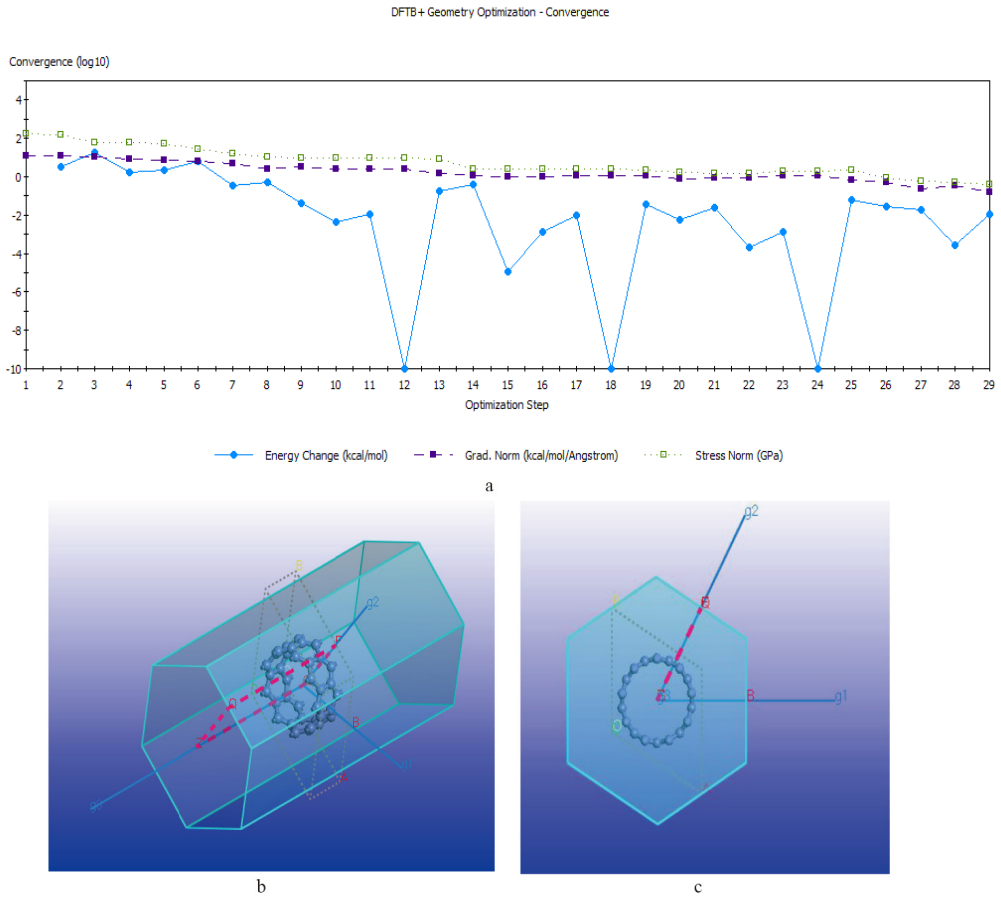

Figure 2. a) Geometry optimization convergence curve. **b)** Optimized geometry- 3D view **c)** optimized geometry- cross-sectionalview.

It can be seen that the structure is the most stable and relaxed when treated with Anderson mixing scheme under standard diagonalization (minimum energy, minimum force and minimum stress) and hence may be expected to produce the best results. Hence, Anderson smearing scheme in combination with standard diagonalization implemented using smart algorithm is strongly recommended for studying Singlewalled Nanotubes.

4.1.2 CASTEP module

In the CASTEP module, electronic minimization of the system was performed using Pulay density mixing treatment of the electrons. Cut-off energy for density mixing was chosen to be 240.0 eV with a charge density mixing g-vector of 1.5/A°. Pseudo-atomic calculations using LDA (CA-PZ), GGA (RPBE), GGA (WC), GGA (PW91) & GGA (PBE-SOL) functionals with an energy tolerance value of 2×10^{-5} eV/atom and maximum force tolerance value of 0.05 eV/A° were performed with a charge spilling parameter for spin component 1 equal to 1.06%. Geometry of the system was optimized with respect to energy change, max. displacement, max. force and max. stress (**Figure 3**).

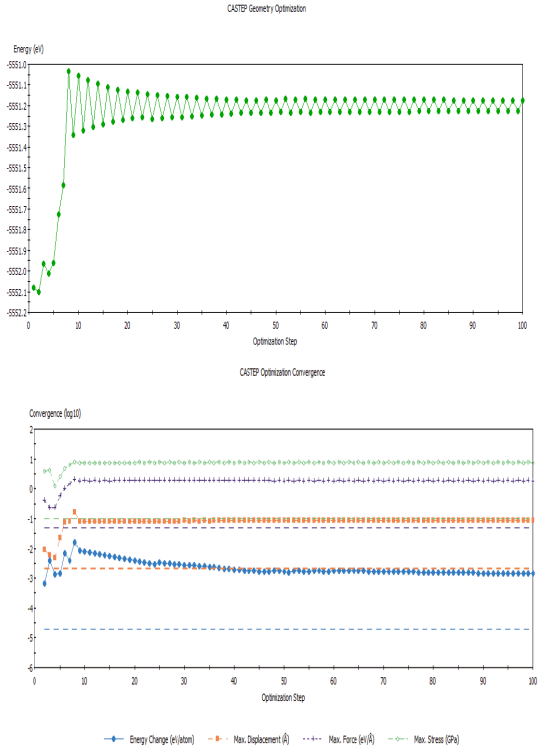

Figure 3. CASTEP geometry optimization **a)** energy evolution **b)** optimization convergence w.r.t. i) energy ii) max. displacement iii) max. force & iv) max. stress.

Ultrasoft pseudo-potential was used in the reciprocal lattice with fixed basis set quality using Gaussian smearing scheme with smearing width of 0.1 eV without any periodic dipole correction. Geometry of the system was optimized using BFGS algorithm implementing variable cell method with geometry line minimiser of tolerance 0.4. Lattice parameters obtained after geometry optimization were a = 10.392983 A°, b = 10.392983 A° & c = 4.260000 A° (Cell Volume = 398.492992 $(A^0)^3$) with cell angles 90°, 90° & 120° confirming the suggested hexagonal geometry (**Figure 4**).

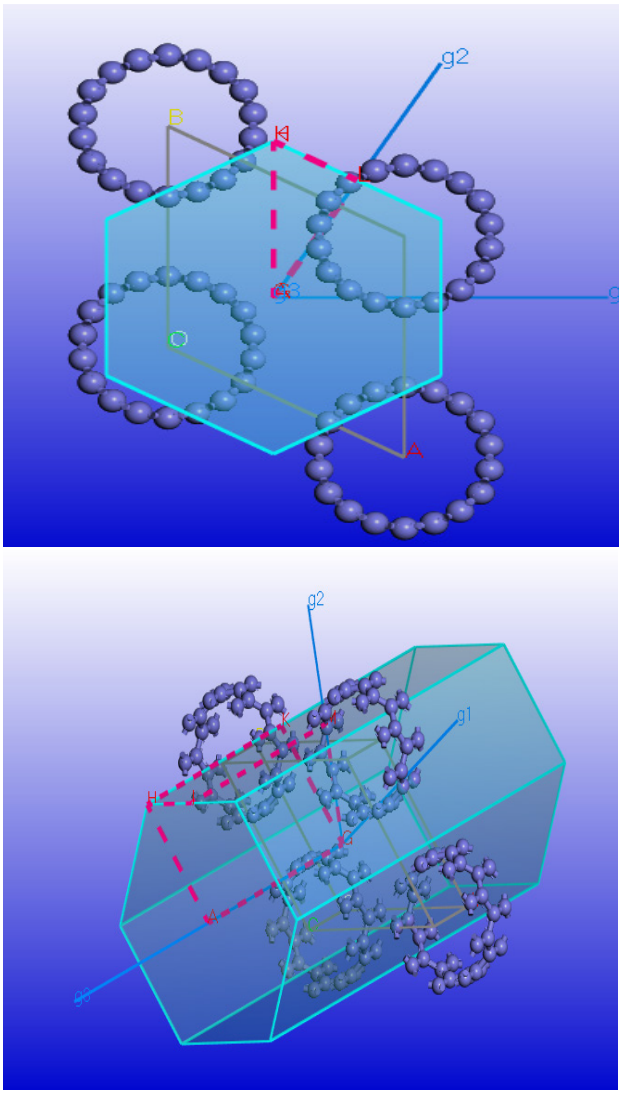

Figure 4. Optimized geometry obtained by supercell approach using CASTEP **a)** lateral view **b)** 3-D view.

The unit chosen comprised of 36 units. As ex-

pected, the first Brullion zone obtained was also hexagonal. Supercell approach was adopted. 6 k-points were chosen for BZ sampling.

4.2 Electronic properties

Continuing with the ground state wavefunctions during the geometry optimization task and the ground state density thus calculated, general k-point calculations for band structure were performed using complex wavefunction with 84 bands per k-point and a band convergence tolerance of 0.1×10^{-4} eV. Fermi energy for the spin-degenerate system with electrical quadrupole moment 0.0332700 Barn was calculated keeping 23 basis set k-points under consideration. General k-point calculations for density of states were also performed treating the system as non-spin-polarized with total energy/atom convergence tolerance value equal to 0.2×10^{-5} eV, all bands spilling parameter for spin component 1 & eigen energy convergence tolerance value equal to 0.8276×10^{-6} eV.

4.2.1 DFTB module

Band Structure and density of states of the optimized structural unit were determined and investigated using smart algorithm without any dispersion correction using various combinations of diagonalization techniques (standard/divide & conquer) and mixing schemes (anderson/broyden/diis/linear) (**Figure 5**). Thermal smearing with smearing parameter equal to 0.005 Hartree was used during all these band structure calculations.

The values of band gap of (9, 0) SWCNT calculated using DFTB Module can be summarized as below:

Table 2. Band gap evaluation using DFTB: (9, 0) Singlewalled Carbon Nanotube

Standard diagonalization				**Divide & conqure diagonalization**			
Anderson	Broyden	Diis	Linear	Anderson	Broyden	Diis	Linear
0.063 eV	0.003 eV	0.005 eV	0.004 eV	0.003 eV	0.003 eV	0.005eV	0.004eV

On the basis of the measurements made by Leiber *et al.* under ultrahigh vacuum conditions at 5 K on a Au (111) substrate, the experimental value of the band gap of (9, 0) SWCNT has been found to be 0.080 eV[48]. By comparing the simulation results with this experimental value, it can be inferred that DFTB module tends to drastically underestimate the band gap value. However, the results obtained with standard diagonalizer and Anderson mixing scheme with mixing parameter 0.05 are comparatively close enough.

4.2.2 CASTEP module

Band Structure and density of states were also

Band structure and density of states of (9,0) SWCNT calculated using density functional tight binding module

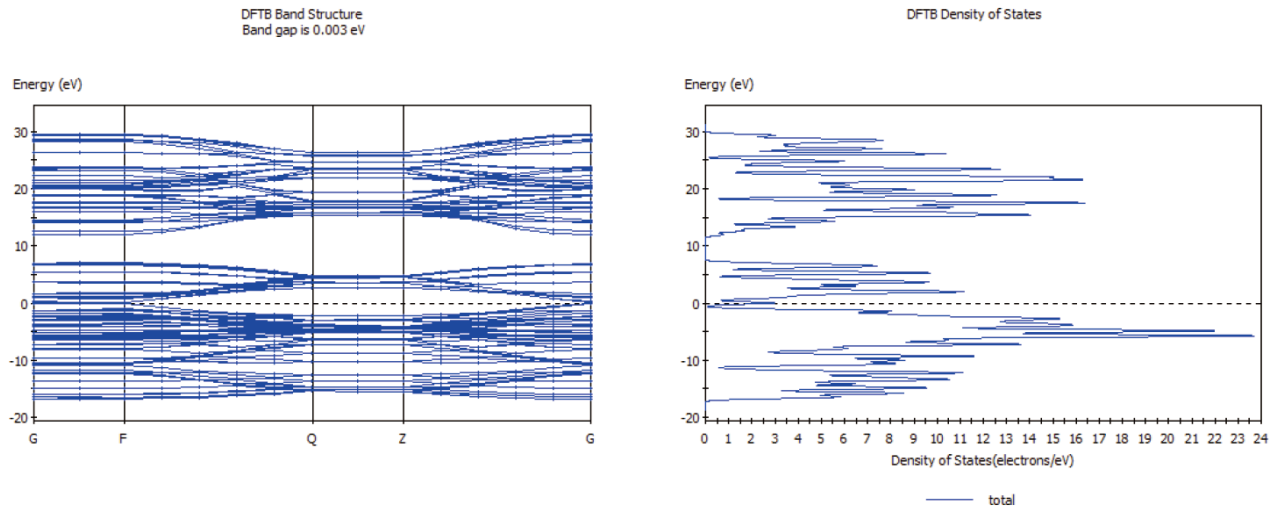

Figure 5a). Band structure deduced with eigen-solver "divide & conquer", mixing scheme—Anderson.

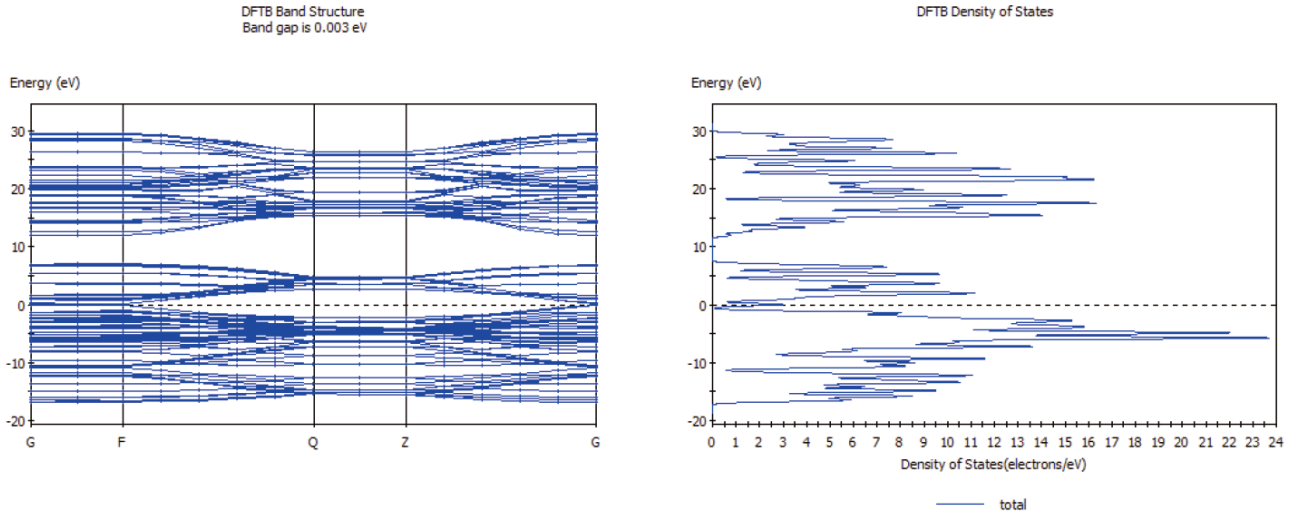

Figure 5b). Band structure deduced with eigen-solver "divide & conquer", mixing scheme—Broyden.

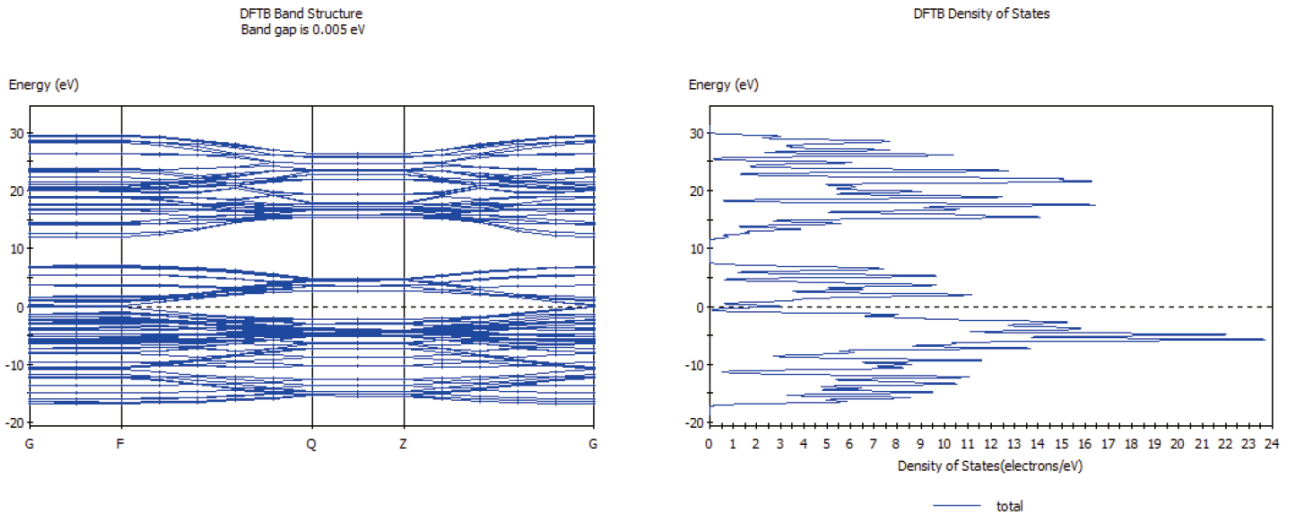

Figure 5c). Band structure deduced with eigen-solver "divide & conquer", mixing scheme—Diis.

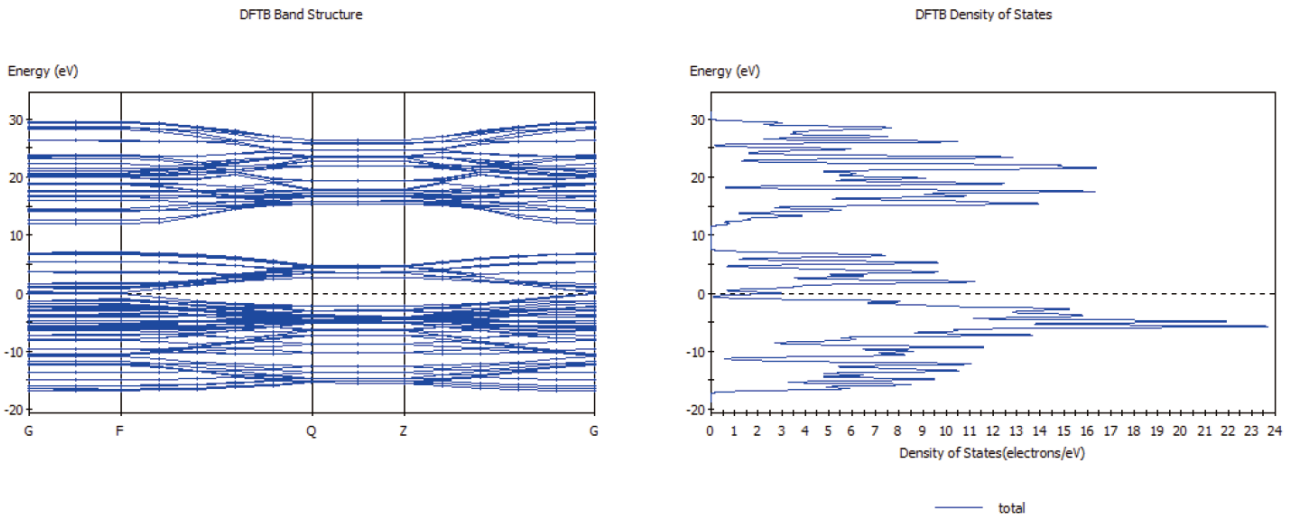

Figure 5d). Band structure deduced with eigen-solver "divide & conquer", mixing scheme—Linear.

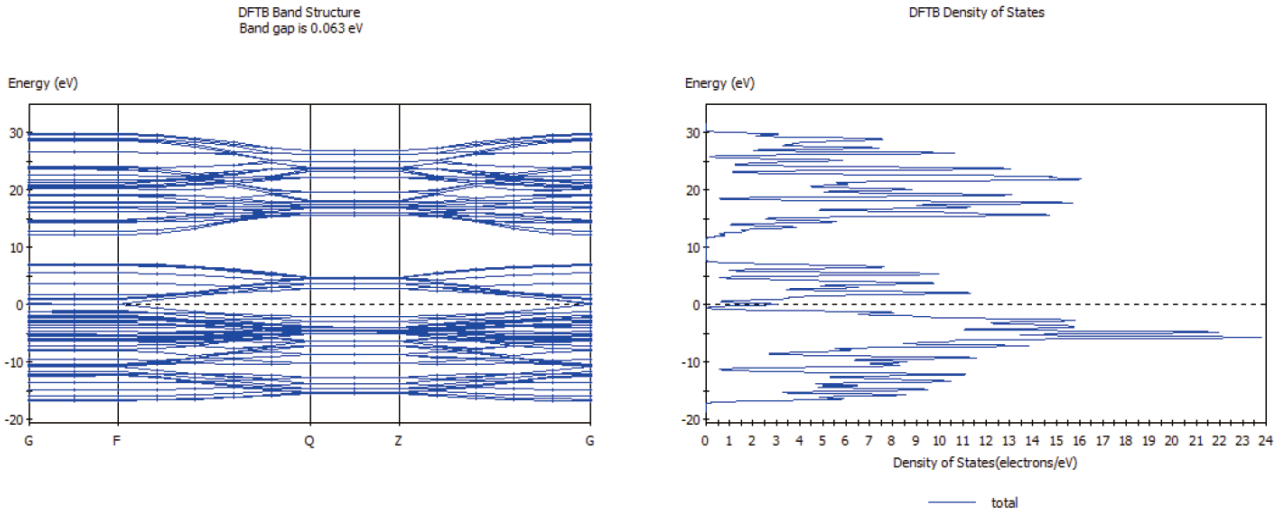

Figure 5e). Band structure deduced with eigen-solver "standard", mixing scheme—Anderson.

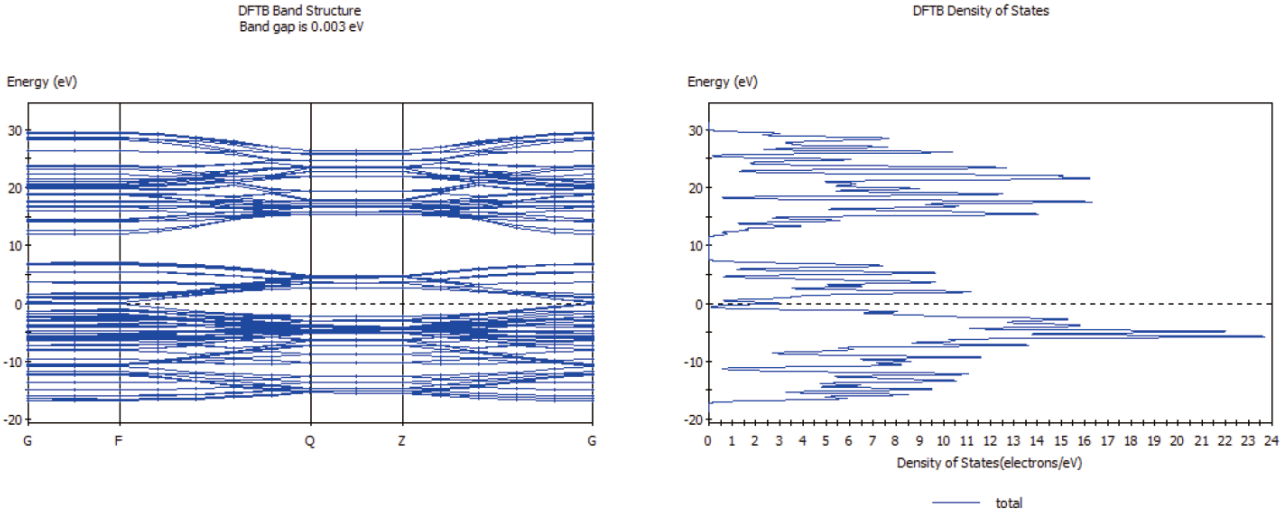

Figure 5f). Band structure deduced with eigen-solver "Standard", mixing scheme—Broyden.

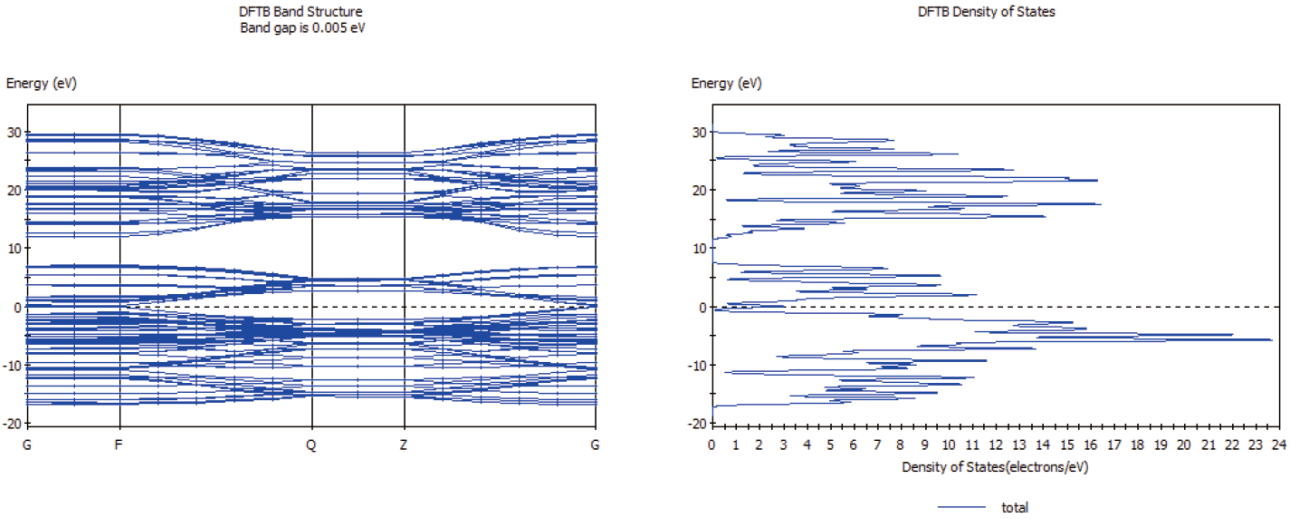

Figure 5g). Band structure deduced with eigen-solver 'Standard', mixing scheme—Diis.

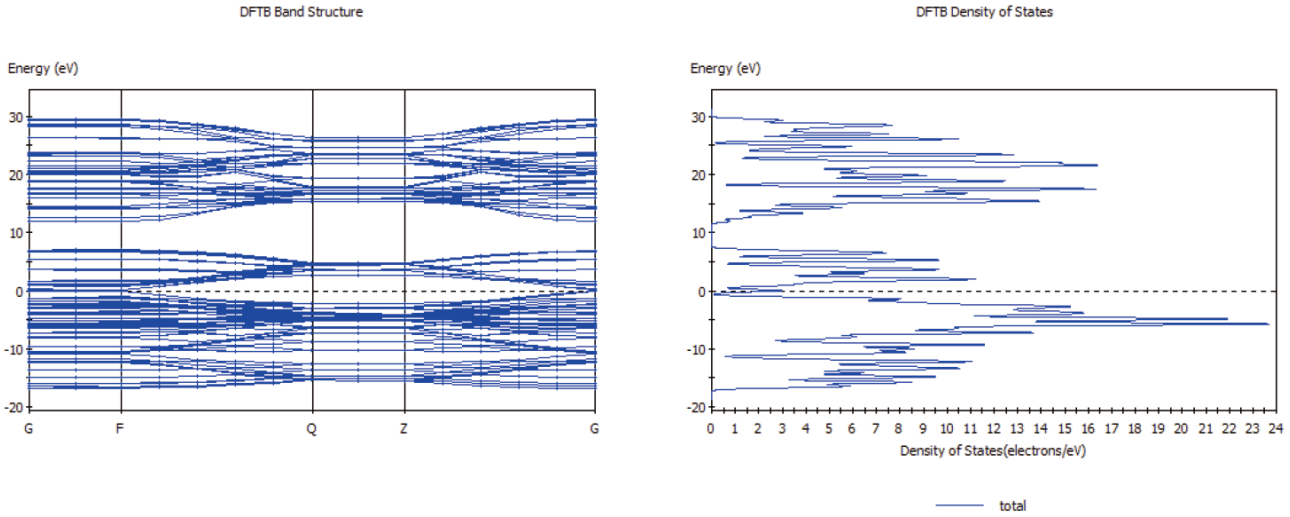

Figure 5h). Band structure deduced with eigen-solver "standard", mixing scheme—Linear.

determined and investigated with the help of the CASTEP module of the software using various available functionals and subfunctionals (**Figure 6**). Fermi energy for the spin-degenerate system with electrical quadrupole moment 0.0332700 Barn was calculated keeping 23 basis set k-points under consideration.

The values of band gap of (9, 0) SWCNT calculated using CASTEP Module can be summarized as below:

Table 3. Band gap evaluation using CASTEP: (9,0) Single-walled Carbon Natotube

LDA	GGA			
CA-PZ	RPBE	PBESOL	WC	PW91
0.190 eV	0.097 eV	0.161 Ev	0.063 eV	0.003 Ev

Comparing these results with the measurements made by Leiber *et al.* (E_g = 0.080 eV), it can be seen that some of the functional-subfunctional combinations in the CASTEP module tend to overestimate the value of the bond gap while others underestimate the value. However, the value of the band gap obtained with GGA functional and RPBE subfunctional is very close to the experimentally observed value. Hence, it can be concluded that GGA-RPBE exchange correlation approximation is the most effective theoretical tool for predicting band gaps in SWCNTs.

As (3 m, 0) SWCNTs are supposed to be of metallic nature, the finite band gap determined theo-

Band structure and density of states of (9,0) SWCNT calculated using CASTEP module

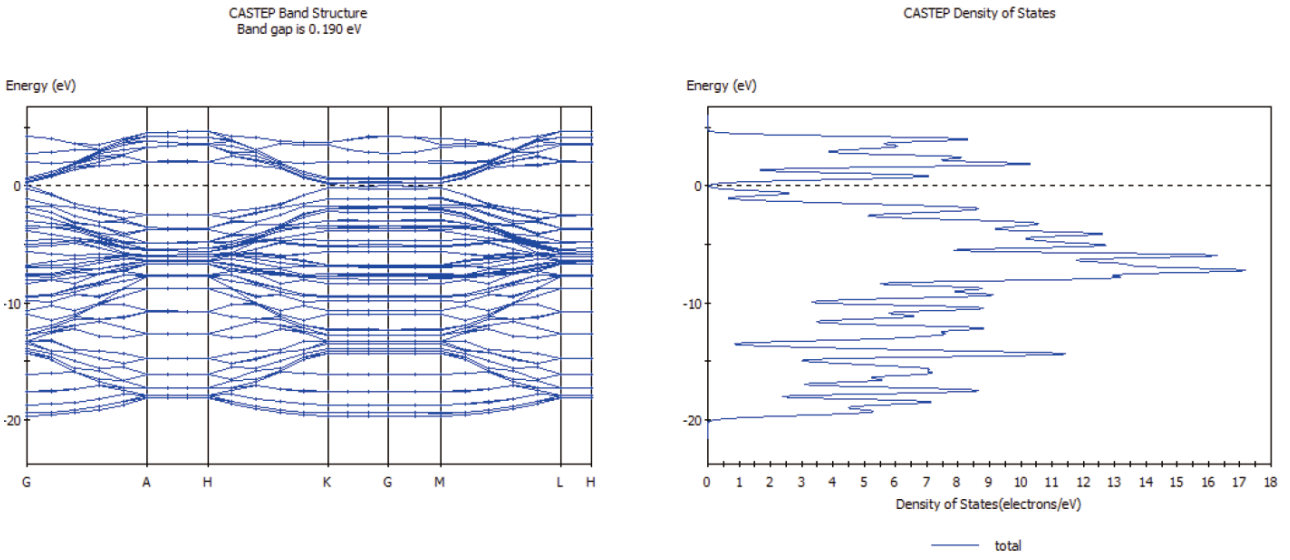

Figure 6a). Band structure deduced with functional—"LDA" and subfunctional—"CA-PZ".

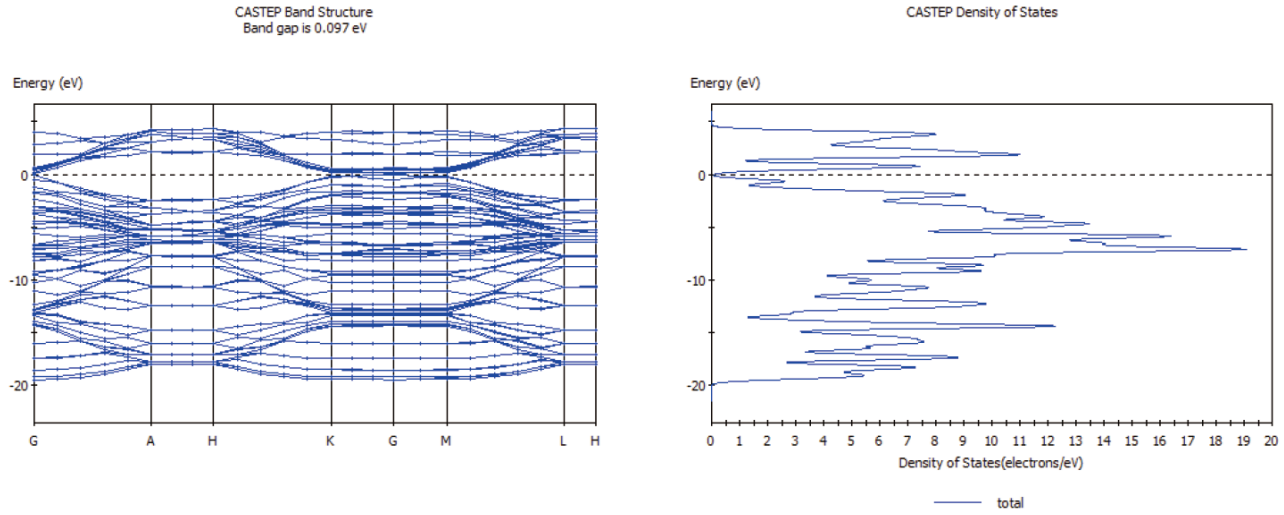

Figure 6b). Band structure deduced with functional—"GGA" and subfunctional—"RPBE".

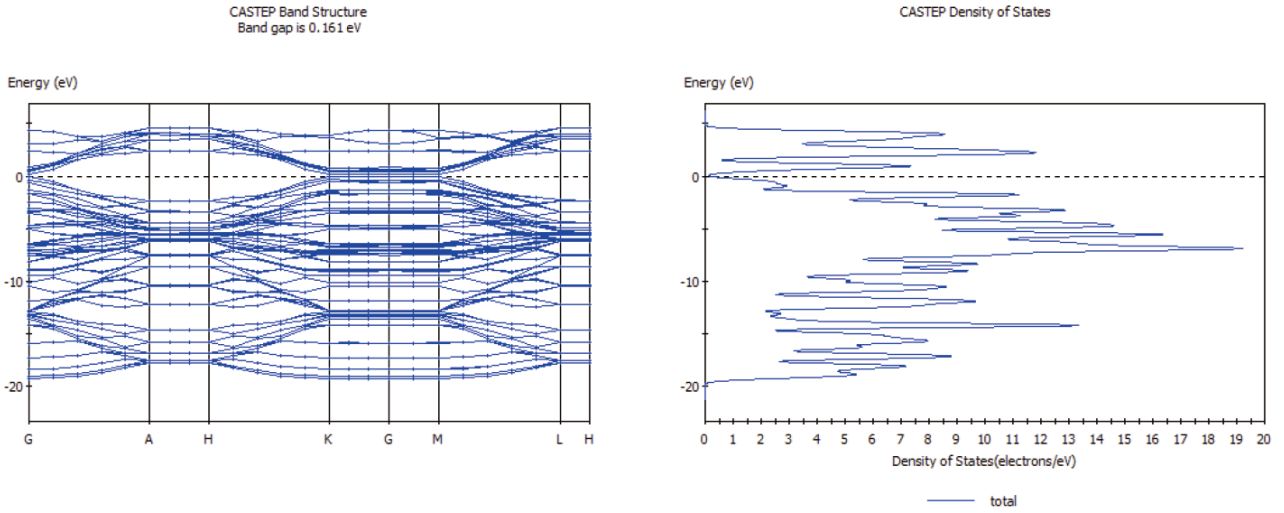

Figure 6c). Band structure deduced with functional—"GGA" and subfunctional—"PBESOL".

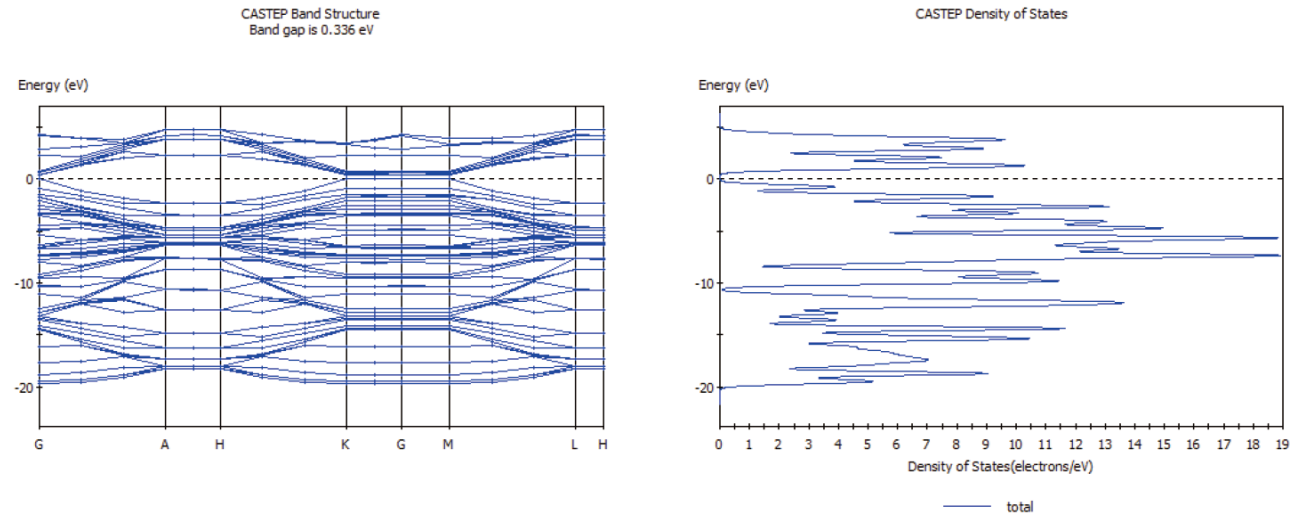

Figure 6d). Band structure deduced with functional—"GGA" and subfunctional—"WC".

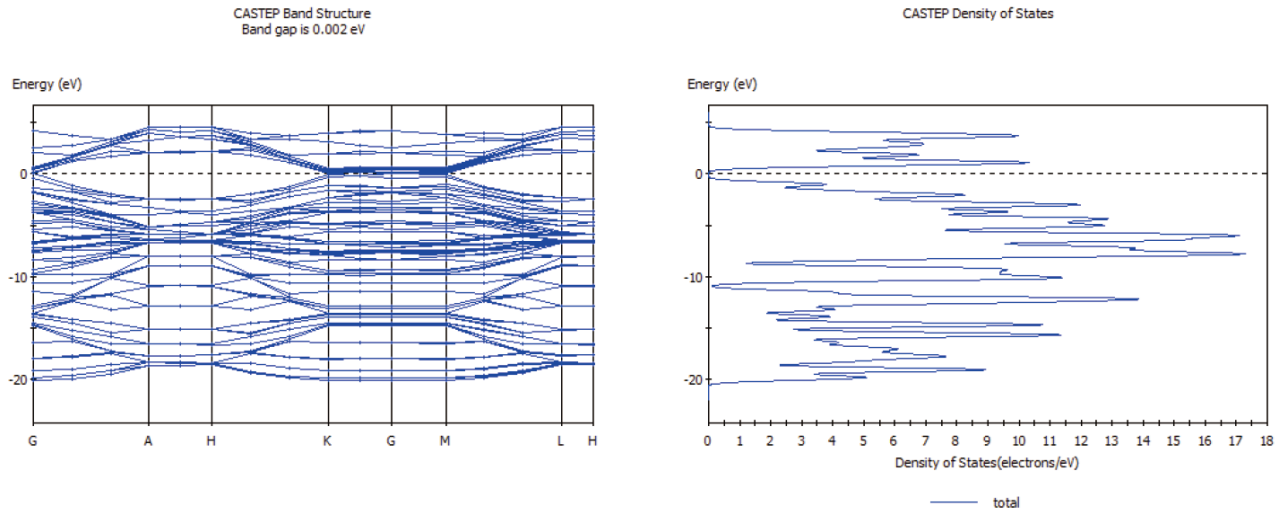

Figure 6e). Band structure deduced with functional—"GGA" and subfunctional—"PW91".

retically (as well as experimentally by Leiber *et al.*) is somewhat unusual. This can however be explained on the basis of σ*-π* hybridization effects caused by the curvature of small-diameter CNTs. In these small CNTs, the π* and σ* states mix and repel each other, leading to lower pure π* states.

4.3 Optical properties

Pseudo atomic calculations performed on C ($2s^2$ $2p^2$) converged in 17 iterations to a total energy of –145.6516 eV. Pulay density mixing treatment with Gaussian smearing was used with finite basis set correction. Partial and full phonon density of states and phonon dispersion curves were determined using linear response phonon calculation (**Figure 7**).

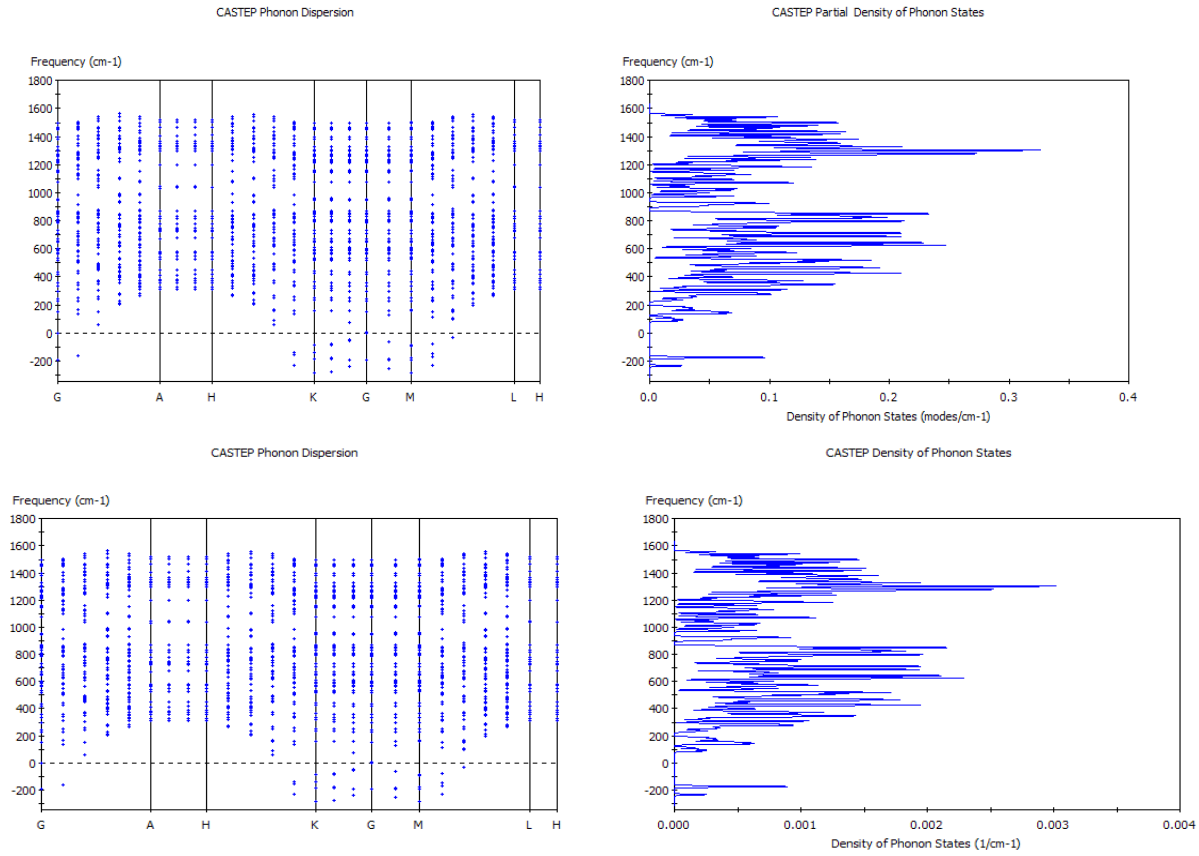

Figure 7. Phonon dispersion w.r.t. **a)** partial phonon density of states **b)** full phonon density of states.

Group theory analysis of eigenvectors reveals that the simulated structure displays Point Group 27: D6h, 6/mmm, 6/m 2/m 2/m symmetries and allows scope for 24 symmetry operations. Frequency calculation at 23 wavevectors was performed using Gonze variational method with TPA preconditioning scheme. The optimized structure was found to belong to the point group 27: D6h, 6/mmm, 6/m 2/m 2/m. with 24 symmetry operations.

Various optical properties of the optimized geometry were investigated using 6 k-point BZ sampling over 84 bands (**Figure 8**).

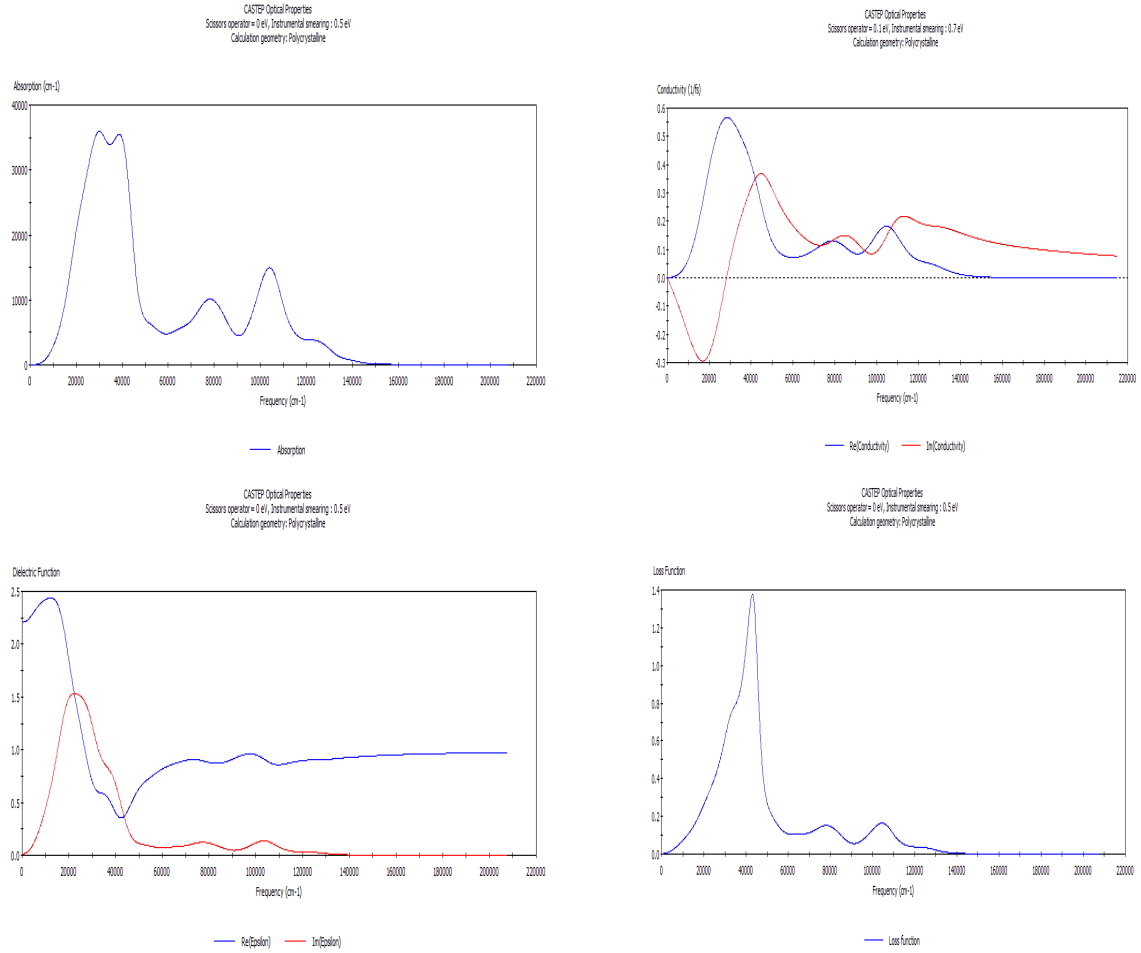

Figure 8. (9, 0) SWCNT: Optical properties **a)** absorption **b)** real & imaginary part of photoconductivity **c)** real & imaginary part of dielectric function **d)** loss function.

From the above curves, the refractive index n and the extinction coefficient k can be easily calculated for any frequency as from the Maxwell's relation:

$$n^* = \varepsilon^{1/2}$$

Here n^* is a complex number. Its real part gives the refractive index n and the imaginary part gives the extinction coefficient k. i.e.

Refractive index $n = Re\ (n^*)$
& Extinction coefficient $k = Im\ (n^*)$

Further, the absorption coefficient α and reflection coefficient R for normally incident radiation of any frequency may also be calculated as:

$$\alpha = 2\omega\kappa/c$$
$$R = |\ (n^* - 1)/\ (n^* + 1)|^{\ 2}$$

where c is the velocity of light. It is clearly evident from the definition that the reflectivity is always positive in the scheduled range of the frequency and is dimensionless. R is sometimes regarded as the index of refraction as a function of the wavelength of light used.

The conductivity $\sigma(\omega)$ is related to the dielectric constant via the relation

$$\sigma(\omega) = \sigma 1 + i\sigma 2 = -i\omega\, 4\pi\, (\varepsilon - 1)$$

The loss function, which is a direct measure of the collective excitations of the systems may be calculated as $Im[-1/\varepsilon]$. Some straightforward algebra may easily reveal that

$$Im[-1/\varepsilon)] = \varepsilon_2 / \varepsilon_1^{\,2} + \varepsilon_2^{\,2}$$

At the plasma frequency, the above expression attains the higher value when $\varepsilon_1 \rightarrow 0$ and $\varepsilon_2 < 1$.

4.4 Thermodynamic properties

Various thermodynamic properties calculated using first principles method through DFTB and CASTEP module of the software have already been discussed in **Table 1**. Also, the variation of Debye temperature with respect to the ambient temperature was determined (**Figure 9a**) for the simulated super-cell structure (**Figure 9b**).

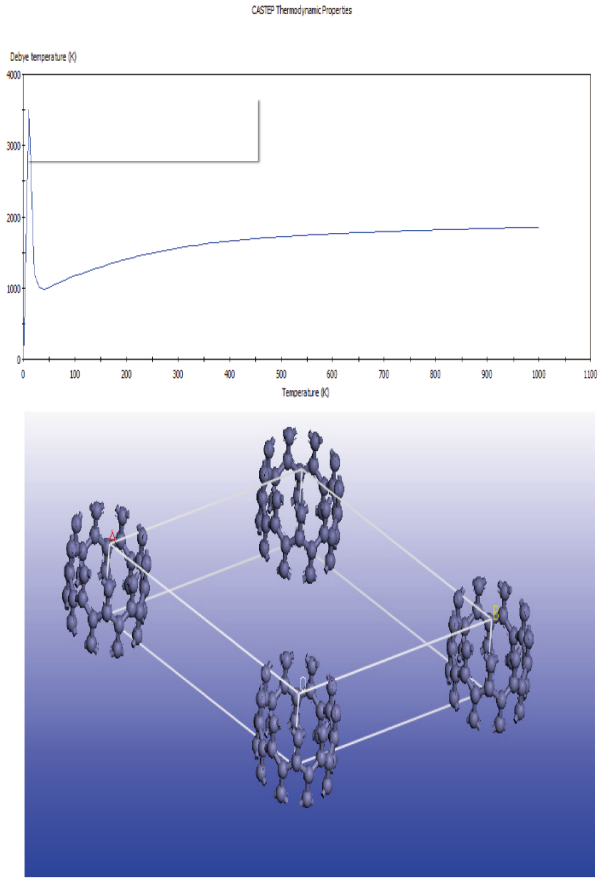

Figure 9. a). Debye temperature Vs Ambient temperature **b)** supercell approach.

It can be seen that the Debye temperature shows striking variations at extremely low temperatures. However, the general formula for the Debye temperature derived from fundamental quantum and thermodynamic assumptions has been very well known as:

$$T_D = \hbar\omega_D / 2\pi\, k_B$$

where ω_D is the Debye frequency and k_B is the Boltzmann constant. Having a casual look at the relation may make one wonder whether temperature dependence of the Debye temperature makes any sense. As per the relation, Debye temperature should rather be independent of the ambient temperature. At this instance, it may be emphasized that the relation arrived at involves various approximations and the Debye temperature has very important physical meaning associated to it, which must be clearly understood.

The maximum energy which can be reached by acoustic thermal vibration of a crystalline solid may be expressed as:

$$U^{max}_{acoustic} = \sum\sum\sum nN_A E^{max}_{acoustic}$$

where $E^{max}_{acoustic}$ is the maximum acoustic thermal vibration energy of an atom. Beyond this energy, interacting or organized lattice vibration does not exist and the thermodynamic behavior of the system is described by independent lattice vibration. The temperature where the collective or acoustic vibration shifts to an independent thermal vibration is the Debye temperature, which can be defined as:

$$T = T_D \quad when \quad U^{max}_{acoustic} = U_{thermal}$$

In other words, Debye temperature is the temperature needed to activate all the phonon modes in a crystal. Thus, higher value of Debye temperature may be associated with stiffness of the material. The strikingly high value of the Debye temperature at extremely low ambient temperature thus points towards exceptional stiffness of the SWCNT under extreme cold conditions. At average room temperature and higher temperatures, it is more or less constant as expected.

5. Conclusions

This first principles study has been performed on (9, 0) Singlewalled Carbon Nanotube and an effort has been made to determine their electronic, optical and thermodynamic properties using CASTEP (Cambridge Sequential Total Energy Package) and DFTB (Density Functional based Tight Binding) modules of the Material Studio Software version 7.0. Various available algorithms, eigen-solvers, diagonalization techniques, density mixing methods, smearing schemes, functionals, subfunctionals have been tried out and their relative efficacy has been adjudged by comparing with the available experimental data. Combination of standard diagonalizer, smart algorithm and Anderson mixing scheme in the DFTB module and the combination of GGA functional and RPBE sub-functional in the CASTEP module have provided fairly good results. These optimized quantum-mechanical calculations not only provide an insight into the structural behaviour of nanomaterials but also present themselves as an effective, convenient and timesaving tool for predicting their physical properties. It may further be mentioned that the unit simulated was a periodic nanostructure (specific tasks on non-periodic structures not covered under the license agreement) and the length of the nanotube simulated was therefore taken at default. Variations in the length may or may not affect the results and need to be further investigated.

Compliance with ethical standards

The authors declare that the integrity of the research has been maintained and the rules of good scientific practice have been duly followed and all the ethical standards of research have been maintained.

Conflict of interest

The authors declare that they have no conflict of interest.

References

1. Iijima S. Helical microtubules of graphitic carbon. Nature 1991; 354: 56–58.
2. Iijima S, Ichihashi T. Single-shell carbon nanotubes of 1-nm diameter. Nature 1993; 363: 603–605.
3. Bethune DS, Johnson RD, Salem JR, *et al.* Atoms in carbon cages: The structure and properties of endohedral fullerenes. Nature 1993; 366: 123–128.
4. Wilson WL, Seabron E, Maclaren S, *et al.* (Invited) Scan-probe microwave reflectance of horizontally aligned arrays of Single-Walled Carbon Nanotubes: Nanoscale imaging of SWNT electrical properties in the Quantum Regime. ECS Meeting Abstracts 2015; 6: 769–769.
5. Park S, Nam JH, Koo JH, *et al.* Enhancement of ambipolar characteristics in single-walled carbon nanotubes using C 60 and fabrication of logic gates. Applied Physics Letters 2015; 106: 103501.
6. Verma P, Saini P, Malik RS, *et al.* Excellent electromagnetic interference shielding and mechanical properties of high loading carbon-nanotubes/polymer composites designed using melt recirculation equipped twin-screw extruder. Carbon 2015; 89: 308–317.
7. Hartmann S, Sturm H, Blaudeck T, *et al.* Experimental and computational studies on the role of surface functional groups in the mechanical behavior of interfaces between single-walled carbon nanotubes and metals. Journal of Materials Science 2015; 50: 1–17.
8. Titova LV, Pint CL, Zhang Q, *et al.* Generation of terahertz radiation by optical excitation of aligned carbon nanotubes. Nano letters 2015; 15: 3267–3272.
9. Battie Y, Broch L, Naciri AE, *et al.* Diameter dependence of the optoelectronic properties of single walled carbon nanotubes determined by ellipsometry. Carbon 2015; 83: 32–39.
10. Sharkey JJ, Stranks SD, Huang J, *et al.* Engineering nanostructures by binding single molecules to single-walled carbon nanotubes. ACS nano 2014; 8: 12748–12754.
11. Vosgueritchian M, Fang Y, Park S, *et al.* High-yield sorting of small-diameter carbon nanotubes for solar cells and transistors. ACS Nano 2014; 8(3): 2609–2617.
12. Bauschlicher Jr CW, Ricca A. Binding of NH_3 to graphite and to a (9, 0) carbon nanotube. Physical Review B 2004; 70(11): 115409.
13. Ricca A, Bauschlicher CW. The physisorption of CH_4

on graphite and on a (9, 0) carbon nanotube. Chemical Physics 2006; 324(2): 455–458.
14. Ricca A, Bauschlicher CW. The adsorption of NO_2 on (9, 0) and (10, 0) carbon nanotubes. Chemical Physics 2006; 323(2): 511–518.
15. Zhang X, Zhao J, Tange M, *et al.* Sorting semiconducting single walled carbon nanotubes by poly (9, 9-dioctylfluorene) derivatives and application for ammonia gas sensing. Carbon 2015; 94: 903–910.
16. Tamburri E, Angjellari M, Tomellini M, *et al.* Electrochemical growth of nickel nanoparticles on carbon nanotubes fibers: Kinetic modeling and implications for an easy to handle platform for gas sensing device. Electrochimica Acta 2015; 157: 115–124.
17. Olney D, Fuller L, Santhanam KSV. Addendum to "A greenhouse gas silicon microchip sensor using a conducting composite with single walled carbon nanotubes". Sensors & Actuators B: Chemical 2014; 203: 942.
18. Dhall S, Jaggi N, Nathawat R. Functionalized multiwalled carbon nanotubes based hydrogen gas sensor. Sensors and Actuators A: Physical 2013; 201: 321–327.
19. Dhall S, Sood K, Jaggi N. A hydrogen gas sensor using a Pt-sputtered MWCNTs/ZnO nanostructure. Measurement Science and Technology 2014; 25: 085103.
20. Cakmak E, Fang X, Yildiz O, *et al.* Carbon nanotube sheet electrodes for anisotropic actuation of dielectric elastomers. Carbon 2015; 89: 113–120.
21. Park S, Park J, Jo I, *et al.* In situ hybridization of carbon nanotubes with bacterial cellulose for three-dimensional hybrid bioscaffolds. Biomaterials 2015; 58: 93–102.
22. Mao H, Kawazoe N, Chen G. Cell response to single-walled carbon nanotubes in hybrid porous collagen sponges. Colloids and Surfaces B: Biointerfaces 2015; 126: 63–69.
23. Sung SJ, Kim T, Yang SJ, *et al.* New insights into the oxidation of single-walled carbon nanotubes for the fabrication of transparent conductive films. Carbon 2015; 81: 525–534.
24. Zhang Z, Geng H, Wang Y, *et al.* Temperature and voltage dependent current–voltage behavior of single-walled carbon nanotube transparent conducting films. Applied Surface Science 2015; 355: 1201–1205.
25. Raïssi M, Vignau L, Cloutet E, *et al.* Soluble carbon nanotubes/phthalocyanines transparent electrode and interconnection layers for flexible inverted polymer tandem solar cells. Organic Electronics 2015; 21: 86–91.
26. Rowell MW, Topinka MA, McGehee MD, *et al.* Organic solar cells with carbon nanotube network electrodes. Applied Physics Letters 2006; 88: 233506.
27. Kahn BE. Patterning Processes for Flexible Electronics. Proceedings of the IEEE 2015; 103: 497–517.
28. Engel M, Steiner M, Seo JWT, *et al.* Hot spot dynamics in carbon nanotube array devices. Nano letters 2015; 15(3): 2127–2131.
29. Bottacchi F, Petti L, Späth F, *et al.* Polymer-sorted (6, 5) single-walled carbon nanotubes for solution-processed low-voltage flexible microelectronics. Applied Physics Letters 2015; 106(19): 193302.
30. Javey A, Guo J, Wang Q, *et al.* Ballistic carbon nanotube field-effect transistors. Nature 2003; 424(6949): 654–657.
31. Sazonova V, Yaish Y, Üstünel H, *et al.* A tunable carbon nanotube electromechanical oscillator. Nature 2004; 431(7006): 284–287.
32. Xu X, Zhai J, Chen Y, *et al.* Well-aligned single-walled carbon nanotubes for optical pulse generation and laser operation states manipulation. Carbon 2015; 95: 84–90.
33. Irita M, Homma Y. Field emission from diameter-defined single-walled carbon nanotubes. Surface and Interface Analysis 2014; 46(12-13): 1282–1285.
34. Payne MC, Teter MP, Allan DC, *et al.* Iterative minimization techniques for ab initio total-energy calculations: Molecular-dynamics and conjugate gradients. Reviews of Modern Physics 1992; 64: 1045–1097.
35. Hohenberg P, Kohn W. Inhomogeneous electron gas. Physics Review 1964; 136: B864–B871.
36. Kohn W, Sham LJ. Self-consistent equations including exchange and correlation effects. Physical Review Journals archive 1965; 140, A1133–A1138.
37. Perdew JP, Zunger A. Self-interaction correction to density-functional approximations for many-electron systems. Physics Review B 1981; 23: 5048–5079.
38. Ceperley DM, Alder BJ. Ground state of the electron

gas by a stochastic method. Physical Review Letters 1980; 45: 566–569.
39. 3Gunnarsson O, Lundqvist BI. Exchange and correlation in atoms, molecules, and solids by the spin-density-functional formalism. Physics Review B 1976; 13: 4274–4298.
40. Perdew JP, Wang Y. Accurate and simple analytic representation of the electron-gas correlation energy. Physics Review B 1992; 45: 13244–13249.
41. Perdew JP, Burke K, Ernzerhof M. Generalized gradient approximation made simple. Physical Review Letters 1995; 77: 3865–3868.
42. Tao J, Perdew JP, Staroverov VN, *et al.* Climbing the density functional ladder: Non-empirical meta-generalized gradient approximation designed for molecules and solids. Physical Review Letters 2003; 91: 146401.
43. Martin R. Electronic structure: Basic theory and practical methods. Cambridge, UK: Cambridge University Press; 2004.
44. Clark SJ, Segall MD, Pickard CJ, *et al.* First principles methods using CASTEP. Zeitschrift für Kristallographie—Crystalline Materials 2005; 220(5-6): 567–570.
45. Blum V, Gehrke R, Hanke F, *et al.* Ab initio molecular simulations with numeric atom-centered orbitals. Computer Physics Communications 2009; 180: 2175–2196.
46. Kresse G, Furthmüller J. Efficient iterative schemes for ab initio total-energy calculations using a plane-wave basis set. Physics Review B 1996; 54: 11169–11186.
47. Segall M, Linda P, Probert M, *et al.* Materials studio CASTEP, version 2.2. Accelrys: San Diego, CA; 2002.
48. Matsuda Y, Tahir-Kheli J, Goddard III WA. Definitive band gaps for single-wall carbon nanotubes. The Journal of Physical Chemistry Letters 2010; 1(19): 2946–2950.